AEROELASTIC DAMPING PREDICTIONS FOR MULTISTAGE TURBOMACHINERY APPLICATIONS

A. Placzek*
*ONERA, Aeroelasticity and Structural Dynamics Department,
29 avenue de la Division Leclerc, F-92322 Châtillon, France

Keywords: CFD; aeroelasticity; turbomachinery; damping; single passage

Abstract

The aeroelastic stability of turbomachinery blade assemblies is usually assessed numerically on isolated blade row configurations although upstream/downstream blade rows can significantly alter the stability. We consider in this paper the influence of a neighboring blade row to compute the generalized aerodynamic forces from which the aeroelastic damping can be evaluated. For that purpose we resort to phase-shifted boundary conditions in the numerical model of a single passage of each blade row to take into account the multiple unsteady phenomena induced by the blade vibration, the blade passage effect of the adjacent blade row and their possible interaction. A Fourier approximation of the global generalized aerodynamic forces of the whole blade is then proposed using the local generalized aerodynamic forces computed on the single blade modeled. An analytic expression of the aeroelastic damping computed with the energy method is finally proposed and the results are compared to those obtained from full annulus reference computations in which all passages are modeled.

1 Introduction

Recent studies [8, 10, 13] have pointed out the importance of modeling adjacent blade rows to improve the evaluation of the aeroelastic stability. Indeed, the relative motion of the different blade rows induces unsteady perturbations which interact with the vibratory excitation of the structure and may increase / decrease significantly the

aeroelastic stability predicted without taking into account adjacent blade rows.

The computation of the 360° full annulus multistage configuration is extremely costly but is however essential to capture accurately the multiple sources of unsteadiness. Specific boundary conditions have therefore been developed since the end of the 70's to reduce the size of the computational domain to a single passage in each blade row. Such boundary conditions rely on the assumption of a space-time periodicity of the flow field that is exploited to prescribe the flow field on a given boundary with respect to the flow field on the opposite boundary using appropriate time phase shifts. These phase shifts arise from the characteristics of the periodic perturbations to propagate and are well known from the spinning modes theory [14, 15].

phase-shifted or "chorochronic" These boundary conditions originally designed by Erdos et al. [5] for a single stage have been used to propagate a single periodic phenomenon (blade passage or blade vibration). A Fourier decomposition of the flow field on the boundaries has then been introduced to avoid the storage of the flow field at many time instants [6, 7]. The boundary conditions have later been extended to handle simultaneously multiple periodic phenomena [7, 11], hence the name of "multiple phase-shifted" or "multichorochronic" boundary conditions. These boundary conditions have recently been implemented in Onera's CFD code elsA and validated on multistage rigid configurations [3] and on the aeroelastic case of a vibrating contrafan [12].

These boundary conditions allow a significant reduction of the computing resources while providing a rather accurate approximation of the pressure distribution on the blade surfaces compared to 360° full annulus reference computations. However the pressure distribution and consequently the generalized aerodynamic forces that are required to assess the aeroelastic stability are computed only on the single passage modeled and the aeroelastic damping of the whole blade row is not directly available. Saiz [13] proposed an expression of the local aerodynamic forces and of the aerodynamic work per cycle due to the vibration perturbation only.

We propose here to further estimate the global generalized aerodynamic forces as the sum of the contributions from each blade and each perturbation under the assumption that the pressure distribution on the blade surface satisfies the same space-time periodicity than the one assumed on the domain boundaries. The missing contributions of the generalized aerodynamic forces on the blades not modeled are then approximated with appropriate phase shifts according to the perturbations considered for the computation. An analytical expression of the damping for the whole blade row is finally established from the Fourier approximation of the generalized aerodynamic forces known on the single blade modeled.

2 Periodicity of the mechanical fields

2.1 Wave form due to the cyclic symmetry

A space-time periodicity of the mechanical variables is assumed because of the cyclic symmetry of the geometry and the loadings. Indeed, the physical domain $\mathscr{D} = \mathscr{D}_F \cup \mathscr{D}_S$ gathering the fluid and structural parts of a given tuned blade row is made up of N_b subdomains for each blade, such that $\mathscr{D}_X = \bigcup_{s=0}^{N_b-1} \mathscr{D}_{X,s}$ with $X \in \{F,S\}$. Each subdomain is identical to the reference domain $\mathscr{D}_{X,0}$ through a rotation of the pitch angle $\beta = 2\pi/N_b$ around the x axis, hence the cyclic symmetry of the geometry. Furthermore the loadings considered here (vibration of the structure and blade passage) also inherit this symmetry since they directly result from the geometry.

As a consequence the mechanical variables w defined in a cylindrical coordinate system are approximated in a very general way as the sum of a finite number N_p of perturbations w_p for which $N_{h,p}$ harmonics $w_{p,k}$ are considered:

$$\boldsymbol{w}(x,r,\theta,t) \approx \sum_{p=1}^{N_p} \sum_{k=0}^{N_{h,p}} \boldsymbol{w}_{p,k}(x,r,\theta,t).$$
 (1a)

Each component $w_{p,k}$ is a spinning mode as described by Tyler and Soffrin [15] such that

$$w_{p,k}(x,r,\theta,t) = c_{p,k}(x,r,\theta)e^{\mathrm{i}k(\kappa_p\theta - \omega_p t)}$$
 (1b)

with the following amplitude

$$c_{p,k}(x,r,\theta) = \sum_{m \in \mathbb{Z}} \check{c}_{p,k,m}(x,r)e^{\mathrm{i}mN_b\theta}.$$
 (1c)

The spinning modes can basically be interpreted as Bloch waves i.e., the product between a steady N_b spatially periodic wave $c_{p,k}(x,r,\theta)$ and a traveling wave $e^{ik(\kappa_p\theta-\omega_pt)}$. Each spinning mode is thus a wave characterized by its pulsation ω_p and its wavenumber κ_p which can be related to a particular perturbation (see [12]).

In the present paper, two primary perturbations are considered, namely the vibration and the blade passage. As a consequence, approximation (1a) with $N_p = 2$ is just a linear superposition of the different perturbations. The nonlinearity of the fluid equations is however likely to generate some interactions between the primary perturbations and therefore to give rise to additional perturbations which should be added in the approximation as extra terms in the sum $(N_p > 2)$. In this way the general approximation (1a) may be used for linear as well as for non-linear systems depending on the type of spinning modes prescribed.

2.2 Phase-shifted boundary conditions

The wave structure of the field approximated with Eqs (1) provides a simple way to obtain the variables on any subdomain $\mathcal{D}_{X,s}$ from the field known on the reference subdomain $\mathcal{D}_{X,0}$. Indeed if $x_s = [x_s, r_s, \theta_s] \in \mathcal{D}_{X,s}$ are the coordinate in a given subdomain such that $x_s = x_0$, $r_s = r_0$ and

 $\theta_s = \theta_0 + s\beta$, the spinning modes are easily deduced from their values known on the reference subdomain with the following transformation involving the phase shift $ks\kappa_n\beta$:

$$\boldsymbol{w}_{p,k}(\boldsymbol{x}_s,t) = \boldsymbol{w}_{p,k}(\boldsymbol{x}_0,t)e^{\mathrm{i}ks\kappa_p\beta} \tag{2}$$

The previous transformation (2) is the cornerstone for the evaluation of aeroelastic damping which is described in section 4.1 since it provides an approximation of the mechanical variables on the missing subdomains which are not modeled.

In practice the approximation (1) is assumed only on the azimuthal boundaries of the reference subdomain $\mathcal{D}_{X,0}$ and leads to the so-called "multichorochronic" or "multiple phase-shifted" boundary conditions which link the spinning modes on a given boundary to their counterpart on the opposite boundary distant from the pitch angle β with a given time shift τ_p :

$$\boldsymbol{w}_{p}(x,r,\theta\pm\beta,t) = \boldsymbol{w}_{p}(x,r,\theta,t\mp\tau_{p})$$
 (3)

The previous transformations (2) and (3) involve the phase shift σ_p which is related to the wave characteristics of the spinning modes as follows:

$$\sigma_p = \kappa_p \beta = \omega_p \tau_p. \tag{4}$$

3 Numerical model of the aeroelastic system

3.1 Structural model

For a linear visco-elastic structure, the approximation (1) still holds. The sum over the harmonics is unnecessary since higher harmonics are related to non-linear phenomena and it can be shown [9, 16] that the general solution for the displacement field u is given by the finite sum of N_b spinning modes, also called traveling waves in the structural dynamics community. The wavenumbers are called the nodal diameters and range from $\kappa_p = 0$ to $\pm N_b/2$ if the blade number N_b is even or to $\pm (N_b - 1)/2$ otherwise.

Since the structural equations are linear, the variational formulation of the problem can be written on the reference subdomain $\mathcal{D}_{S,0}$ only and leads to a system of decoupled equations for each traveling wave [16]. The Finite Element discretization of the problem yields:

$$\mathbf{M}\ddot{\mathbf{u}}_p + \mathbf{C}\dot{\mathbf{u}}_p + \mathbf{K}\mathbf{u}_p = \mathbf{f}_{a,p}(\mathbf{u}_p, \dot{\mathbf{u}}_p) \quad (5)$$

where **M** is the mass matrix, **K** is the stiffness matrix including the centrifugal effects and **C** is the damping and gyroscopic effect matrix. The right-hand side of Eq (5) stands for the aerodynamic forces exerted by the pressure on the reference blade's fluid-structure interface Γ_0 :

$$\mathbf{f}_{a,p}(\mathbf{u}_p, \dot{\mathbf{u}}_p, t) = p(\mathbf{u}_p, \dot{\mathbf{u}}_p, t) \, \mathbf{n}. \tag{6}$$

The displacement field on the boundaries satisfies the chorochronic relation (3) and can also be written $u_p(\theta + \beta, t) = u_p(\theta, t) e^{i\sigma_p}$ since higher harmonics are not considered.

The vibratory behavior of the structure is described for small amplitudes of vibration by the eigenmodes defined as the solution of $\mathbf{K} \varphi_p^{(i)} - \omega_p^{(i)2} \mathbf{M} \varphi_p^{(i)} = \mathbf{0}$ with the additional constraint of chorochronicity $\varphi_p^{(i)}(\theta + \beta) = \varphi_p^{(i)}(\theta) e^{\mathbf{i} \sigma_p}$. Each mode type $\varphi_p^{(i)}$ for $i = 1, \ldots, n_m$ has N_b different spatial patterns depending on the wavenumber κ_p . The complex chorochronicity condition produces complex conjugate pairs of eigenmodes with the same eigenvalues. The eigenmodes inherit the cyclic symmetry property and are defined on any subdomain $\mathscr{D}_{S,s}$ with the relation

$$\varphi_p^{(i)}(x_s) = \varphi_p^{(i)}(x_0) e^{is\sigma_p}.$$
(7)

3.2 Fluid model

The fluid flow is governed by the nonlinear Unsteady Reynolds Averaged Navier-Stokes equations which prevent obtaining decoupled equations for each spinning mode like for the structure. The equations are therefore solved for the aerodynamic variables \boldsymbol{W} which are approximated by Eq (1) on some of the domain boundaries only. The equations in the rotating frame of reference of each blade row write with the arbitrary Lagrangian-Eulerian formulation

$$\frac{\mathrm{d}}{\mathrm{d}t} \int_{\mathscr{D}_F} \mathbf{W} \, \mathrm{d}v + \oint_{\partial \mathscr{D}_F} (\mathbf{F}^C + \mathbf{F}^D) \cdot \mathbf{n} \, \mathrm{d}s = \int_{\mathscr{D}_F} \mathbf{S} \, \mathrm{d}v \quad (8)$$

with W the vector of the conservative and turbulent variables, F^C and F^D the convective and diffusive fluxes and S a source term containing the gyroscopic effects due to the rotation. The fluxes and the source term are supplemented by appropriate terms accounting for the Spalart-Allmaras

turbulence model considered here. In the framework of the arbitrary Lagrangian-Eulerian formulation, the convective fluxes are altered by a relative mesh deformation velocity v_d which matches the velocity of the blade induced by the vibration at the fluid-structure interface Γ .

The no-slip boundary conditions applied on the hub, the carter and the blade surfaces force the relative velocity of the flow to match the relative wall velocity $v = v_w - \Omega r i_\theta$ where Ω is the constant rotation speed of the blade row. The wall velocity v_w is equal to the rotation speed $\Omega r i_\theta$ if the wall is rigid and rotates (hub); it is equal to zero if the wall is rigid and not rotating (carter) and is equal to the sum of the rotation speed and the deformation velocity $v_d + \Omega r i_\theta$ if the wall rotate and is flexible (blades).

Subsonic injection and pressure boundary conditions are prescribed respectively on the inlet and outlet planes of the fluid domain. Full annulus 360° simulations performed on the whole domain \mathcal{D}_F use matching joins on the azimuthal boundaries of each passage and a sliding plane boundary condition is applied at the interface between the blade rows. On these boundaries, single passage simulations performed on the reference subdomain $\mathcal{D}_{F,0}$ require contrarily multiple phase-shifted boundary conditions which have been described in section 2.2.

The flow equations are discretized with a Finite Volume technique. The fluxes are approximated by the 2^{nd} order Roe's scheme with Van Albada's limiter and Harten entropic correction. The time integration combines the implicit backward Euler scheme and the 2^{nd} order Gear's method which solves the subiterations in physical time-step. See [1] for more details about the CFD solver *elsA*.

3.3 Aeroelastic coupling strategy

A "weak" coupling strategy is considered here, meaning that a harmonic displacement is prescribed to the blade so that the structural equations Eqs (5) have not to be solved at each time step. A single mode shape $\varphi_{n_d} = \varphi_{p_0}^{(i_0)}$ for a given value of the nodal diameter $\kappa_{p_0} = n_d$ and the pulsation $\omega_0 = \omega_{p_0}^{(i_0)}$ is selected and the prescribed

motion is therefore defined with a maximal amplitude q^* and an initial phase Ψ by

$$\mathbf{u}_{\text{pres}}(\mathbf{x}_s, t) = \Re \left\{ \boldsymbol{\varphi}_{n_d}(\mathbf{x}_0) \, q^* e^{\mathrm{i}(s\boldsymbol{\sigma}_{n_d} - \boldsymbol{\omega}_0 t - \boldsymbol{\Psi})} \right\}. \tag{9}$$

In this way the structural displacement (9) is a single traveling wave coordinate $u_{\text{pres}} = u_{p_0}$ and satisfies necessarily the chorochronic property. The time derivative of this displacement defines the deformation velocity $v_d(\Gamma,t) = \dot{u}_{\text{pres}}(\Gamma,t)$ of the fluid-structure interface $\Gamma = \bigcup_{s=0}^{N_b-1} \Gamma_s$ which is used for the wall boundary condition of the fluid problem. The deformation of the fluid-structure interface Γ is then propagated inside the fluid domain \mathcal{D}_F using a structural analogy [4].

4 Aeroelastic damping definition

Following Carta's energy method [2], the aeroelastic damping is defined as the ratio of the aero-dynamic work W_a and the maximal structural kinetic energy $\mathscr{E}_{\rm kin}^* = (\overline{\boldsymbol{\varphi}}_{n_d}^{\mathsf{T}} \mathbf{M} \boldsymbol{\varphi}_{n_d}) q^{*2}/2$:

$$\alpha = -\frac{W_a}{4\pi \mathcal{E}_{\rm kin}^*}.\tag{10}$$

The aerodynamic work on a vibration cycle is computed as the inner product between the structural velocity $\dot{\boldsymbol{u}}_{\text{pres}}$ and the aerodynamic force \boldsymbol{f}_a :

$$W_a(t_0) = -\omega_0 q^* \int_{t_0}^{t_0 + T_0} \widetilde{W}_a(t) dt \qquad (11)$$

with the following definitions of the integrand

$$\widetilde{W}_{a}(t) = f_{\text{ag}}^{\mathfrak{R},\Gamma}(t)\sin(\omega_{0}t + \Psi) + f_{\text{ag}}^{\mathfrak{I},\Gamma}(t)\cos(\omega_{0}t + \Psi)$$
(12)

and the global generalized aerodynamic forces:

$$f_{ag}^{\mathfrak{R},\Gamma}(t) = \sum_{s=0}^{N_b-1} \boldsymbol{\varphi}^{\mathfrak{R}}(\boldsymbol{x}_s) \cdot \boldsymbol{f}_a(\boldsymbol{x}_s,t), \quad (13a)$$

$$f_{ag}^{\mathfrak{I},\Gamma}(t) = -\sum_{s=0}^{N_b-1} \boldsymbol{\varphi}^{\mathfrak{I}}(\boldsymbol{x_s}) \cdot \boldsymbol{f_a}(\boldsymbol{x_s},t). \quad (13b)$$

4.1 Global generalized aerodynamic forces approximation

An estimation of the global generalized aerodynamic forces components $f_{ag}^{\Re,\Gamma}$ and $f_{ag}^{\Im,\Gamma}$ can

be obtained using the chorochronicity property of the structural eigenmode and of the pressure field. Indeed, Eq (7) leads to:

$$\varphi_{n_d}^{\Re}(\boldsymbol{x}_s) = \varphi_{n_d}^{\Re}(\boldsymbol{x}_0)\cos(s\boldsymbol{\sigma}_{n_d})$$

$$-\varphi_{n_d}^{\Im}(\boldsymbol{x}_0)\sin(s\boldsymbol{\sigma}_{n_d})$$

$$\varphi_{n_d}^{\Im}(\boldsymbol{x}_s) = \varphi_{n_d}^{\Re}(\boldsymbol{x}_0)\sin(s\boldsymbol{\sigma}_{n_d})$$

$$+\varphi_{n_d}^{\Im}(\boldsymbol{x}_0)\cos(s\boldsymbol{\sigma}_{n_d})$$

$$(14a)$$

and taking the real part of the approximation Eq (1) for the pressure field leads to:

$$p(\boldsymbol{x}_{s},t) \approx \sum_{p=1}^{N_{p}} \sum_{k=0}^{N_{h,p}} a_{p,k}[p(\boldsymbol{x}_{s})] \cos(k\omega_{p}t) +b_{p,k}[p(\boldsymbol{x}_{s})] \sin(k\omega_{p}t)$$
(15)

with the following Fourier coefficients defined from the pressure on the reference passage only:

$$a_{p,k}[p(\mathbf{x}_s)] = a_{p,k}[p(\mathbf{x}_0)]\cos(ks\sigma_p)$$
 (16a)
$$-b_{p,k}[p(\mathbf{x}_0)]\sin(ks\sigma_p)$$

$$b_{p,k}[p(\mathbf{x}_s)] = a_{p,k}[p(\mathbf{x}_0)]\sin(ks\sigma_p)$$

$$+ b_{p,k}[p(\mathbf{x}_0)]\cos(ks\sigma_p)$$
(16b)

Since the generalized aerodynamic forces are computed from the pressure field, the same type of approximation holds with the notation $\mathfrak{C} = \mathfrak{R}$ or \mathfrak{I} to designate the real or imaginary part:

$$f_{ag}^{\mathfrak{C},\Gamma}(t) \approx \sum_{p=1}^{N_p} \sum_{k=0}^{N_{h,p}} a_{p,k} [f_{ag}^{\mathfrak{C},\Gamma}] \cos(k\omega_p t) + b_{p,k} [f_{ag}^{\mathfrak{C},\Gamma}] \sin(k\omega_p t).$$

$$(17)$$

However the forces are computed only on the fluid-structure interface Γ_0 of the reference passage $\mathcal{D}_{F,0}$ and the Fourier coefficients $a_{p,k}[f_{ag}^{\mathfrak{C},\Gamma}]$ and $b_{p,k}[f_{ag}^{\mathfrak{C},\Gamma}]$ of the global generalized aerodynamic forces have to be evaluated from the coefficients of the local generalized aerodynamic forces given by

$$a_{p,k}[f_{ag}^{\mathfrak{C},\Gamma_0}] = \int_{\Gamma_0} \boldsymbol{\varphi}^{\mathfrak{C}}(\boldsymbol{x}_0) \cdot a_{p,k}[p(\boldsymbol{x}_0)] \boldsymbol{n} ds, \quad (18a)$$

$$b_{p,k}[f_{ag}^{\mathfrak{C},\Gamma_0}] = \int_{\Gamma_0} \boldsymbol{\varphi}^{\mathfrak{C}}(\boldsymbol{x}_0) \cdot b_{p,k}[p(\boldsymbol{x}_0)] \boldsymbol{n} ds. \tag{18b}$$

Introducing the approximations (14) and (15) for the structural mode and the pressure in the decompositions (13a) and (13b) of real and imaginary parts of the generalized aerodynamic forces leads to an expression within which the Fourier coefficients of the local generalized aerodynamic forces $a_{p,k}[f_{ag}^{\mathfrak{C},\Gamma_0}]$ and $b_{p,k}[f_{ag}^{\mathfrak{C},\Gamma_0}]$ are weighted by two sums over trigonometric functions, namely $\sum_{s=0}^{N_b-1}\cos[s(\sigma_{n_d}\pm k\sigma_p)]$ and $\sum_{s=0}^{N_b-1}\sin[s(\sigma_{n_d}\pm k\sigma_p)]$. The following wavenumber and phase shift therefore appear naturally

$$\mathfrak{K}_{p,k}^{\pm} = n_d \pm k \kappa_p, \tag{19a}$$

$$\mathfrak{S}_{p,k}^{\pm} = \sigma_{n_d} \pm k \sigma_p = \mathfrak{K}_{p,k}^{\pm} \beta. \tag{19b}$$

The previous sums of trigonometric functions are developed with complex exponentials which are interpreted as geometric progressions with the common ratio $\pm \mathfrak{S}_{p,k}^{\pm}$. These progressions vanish except when $\mathfrak{K}_{p,k}^{\pm} \equiv 0 \pmod{N_b}$ in which case $\sum_{s=0}^{N_b-1} e^{\pm is\mathfrak{S}_{p,k}^{\pm}} = N_b$. As a consequence the sum over the sines always vanishes and the sum over the cosines is a Dirac comb \coprod_{N_b} :

$$\sum_{s=0}^{N_b-1} \cos(s\mathfrak{S}_{p,k}^{\pm}) = \coprod_{N_b} (\mathfrak{K}_{p,k}^{\pm})$$

$$= \sum_{n \in \mathbb{Z}} N_b \delta(\mathfrak{K}_{p,k}^{\pm} - nN_b).$$
(20)

After rearrangement of the terms, the Fourier coefficients of the real part of the global generalized aerodynamic force can easily be determined from their counterparts computed locally on Γ_0 :

$$a_{p,k}[f_{ag}^{\mathfrak{R},\Gamma}] = a_{p,k}[f_{ag}^{\mathfrak{R},\Gamma_0}] \left\{ \coprod_{N_b}(\mathfrak{K}_{p,k}^+) + \coprod_{N_b}(\mathfrak{K}_{p,k}^-) \right\} + b_{p,k}[f_{ag}^{\mathfrak{I},\Gamma_0}] \left\{ \coprod_{N_b}(\mathfrak{K}_{p,k}^-) - \coprod_{N_b}(\mathfrak{K}_{p,k}^+) \right\}$$
(21a)

$$b_{p,k}[f_{ag}^{\mathfrak{R},\Gamma}] = b_{p,k}[f_{ag}^{\mathfrak{R},\Gamma_0}] \Big\{ \coprod_{N_b} (\mathfrak{K}_{p,k}^+) + \coprod_{N_b} (\mathfrak{K}_{p,k}^-) \Big\}$$
$$-a_{p,k}[f_{ag}^{\mathfrak{I},\Gamma_0}] \Big\{ \coprod_{N_b} (\mathfrak{K}_{p,k}^-) - \coprod_{N_b} (\mathfrak{K}_{p,k}^+) \Big\}$$
(21b)

The same type of relations can be established for the imaginary part of the generalized aero-dynamic forces, thus yielding the coefficients $a_{p,k}[f_{ag}^{\mathfrak{I},\Gamma}]$ and $b_{p,k}[f_{ag}^{\mathfrak{I},\Gamma}]$ as a linear combination of the local Fourier coefficients $a_{p,k}[f_{ag}^{\mathfrak{C},\Gamma_0}]$ and $a_{p,k}[f_{ag}^{\mathfrak{C},\Gamma_0}]$.

4.2 Expression of the aerodynamic work for quasi-periodic signals

Once the global generalized aerodynamic forces of the whole blade row are known from the previous expressions, the aerodynamic work defined by Eqs (11) and (12) can be evaluated.

As a preliminary remark we mention the particular case of generalized aerodynamic forces governed exclusively by the vibration frequency ω_0 (and possibly some harmonics) which write $f_{ag}^{\mathfrak{C},\Gamma} = \sum_{k=0}^{N_h} a_k^{\mathfrak{C},\Gamma} \cos(k\omega_0 t) + b_k^{\mathfrak{C},\Gamma} \cos(k\omega_0 t)$ with the shorthand notation $a_k^{\mathfrak{C},\Gamma} = a_k[f_{ag}^{\mathfrak{C},\Gamma}]$ and $b_k^{\mathfrak{C},\Gamma} = b_k[f_{ag}^{\mathfrak{C},\Gamma}]$. The aerodynamic work is then easily derived analytically as $W_a = -\pi q^*[(a_1^{\mathfrak{R},\Gamma} - b_1^{\mathfrak{R},\Gamma})\sin\Psi + (a_1^{\mathfrak{R},\Gamma} + b_1^{\mathfrak{R},\Gamma})\cos\Psi]$ and the expression is independent of the initial time instant t_0 .

Such an expression is useful for computations on an isolated flexible blade row in which case the generalized aerodynamic forces involve the sole vibration frequency (and some harmonics). This is however no longer the case when the generalized aerodynamic forces are approximated more generally by the expression Eq (17) which is necessary when multiple perturbations are involved. To address this problem, a mean value of the aerodynamic work is first proposed as the limit for an infinitely long time interval:

$$\overline{W}_a(t_0) = \lim_{\tau \to \infty} -\frac{2\pi q^*}{\tau} \int_{t_0}^{t_0 + \tau} \widetilde{W}_a(t) dt.$$
 (22)

In this way the mean aerodynamic work is independent of the initial time instant t_0 . Indeed it can be shown using the approximation of the generalized aerodynamic forces Eq (17) that the analytical expression is given by:

$$\overline{W}_{a} = -\pi q^{*} \sum_{p=1}^{N_{p}} \sum_{k=0}^{N_{h,p}} \left[(a_{p,k}^{\mathfrak{R},\Gamma} - b_{p,k}^{\mathfrak{I},\Gamma}) \sin \Psi + (a_{p,k}^{\mathfrak{I},\Gamma} + b_{p,k}^{\mathfrak{R},\Gamma}) \cos \Psi \right] \delta_{p,k}.$$

$$(23)$$

The previous expression generalizes the one given above for a single fundamental frequency by means of the Dirac delta function $\delta_{p,k} = \delta(\omega_0 - k\omega_p)$. The mean aerodynamic work is therefore a measure of the work done by the component of the generalized aerodynamic forces

whose frequency is identically equal to the vibration frequency ω_0 .

When multiple perturbations contribute to the aeroelastic response, the aerodynamic work W_a on a vibration cycle is no longer constant and depends on the initial time instant t_0 . An analytic expression of the (instantaneous) aerodynamic work is derived using the approximation Eq (17) of the generalized aerodynamic forces:

$$W_{a}(t_{0}) = -\omega_{0}q^{*} \sum_{p=1}^{N_{p}} \sum_{k=1}^{N_{h,p}} \left[A_{p,k}^{0} + A_{p,k}^{+} \cos \Omega_{p,k}^{+}(t_{0}) + B_{p,k}^{+} \sin \Omega_{p,k}^{+}(t_{0}) + A_{p,k}^{-} \cos \Omega_{p,k}^{-}(t_{0}) + B_{p,k}^{-} \sin \Omega_{p,k}^{-}(t_{0}) \right]$$
(24)

with $\Omega_{p,k}^{\pm}(t_0) = \omega_{p,k}^{\pm}t_0 + \Psi$, $\omega_{p,k}^{\pm} = \omega_0 \pm k\omega_p$ and the following definitions of the coefficients:

$$A_{p,k}^{0} = (\lambda_{p,k}^{-} \sin \Psi + \eta_{p,k}^{-} \cos \Psi) \delta_{p,k} T_{0}$$
 (25a)

$$A_{p,k}^{\pm} = \frac{1 - \delta_{p,k}}{\omega_{p,k}^{\pm}} \left[\lambda_{p,k}^{\pm} \left(1 - \cos(\omega_{p,k}^{\pm} T_0) \right) + \eta_{p,k}^{\pm} \sin(\omega_{p,k}^{\pm} T_0) \right],$$
(25b)

$$B_{p,k}^{\pm} = \frac{1 - \delta_{p,k}}{\omega_{p,k}^{\pm}} \left[\eta_{p,k}^{\pm} \left(\cos(\omega_{p,k}^{\pm} T_0) - 1 \right) + \lambda_{p,k}^{\pm} \sin(\omega_{p,k}^{\pm} T_0) \right],$$
(25c)

$$\lambda_{p,k}^{\pm} = \left(a_{p,k} [f_{ag}^{\mathfrak{R},\Gamma}] \pm b_{p,k} [f_{ag}^{\mathfrak{I},\Gamma}] \right) / 2, \qquad (25d)$$

$$\eta_{p,k}^{\pm} = \left(a_{p,k}[f_{ag}^{\mathfrak{I},\Gamma}] \mp b_{p,k}[f_{ag}^{\mathfrak{R},\Gamma}]\right)/2.$$
(25e)

The aerodynamic work is thus a quasiperiodic function and fluctuates in an interval $[W_a^{\min}; W_a^{\max}]$ centered around a mean value which converges to the mean value \overline{W}_a in the sense of Eq (22). Indeed it may be shown that $\overline{W}_a = -\omega_0 q^* \sum_{p,k} A_{p,k}^0$. The extrema of the function are hard to find analytically in the general case and are therefore estimated numerically from the evaluation of the aerodynamic work on a very long time interval which is possible thanks to the Fourier approximation proposed here. The CFD simulations are indeed very time consuming and the generalized aerodynamic forces are evaluated only on a small time interval which may be insufficient to reach accurately the extrema.

The mean value \overline{W}_a of the work and the extrema W_a^{\min} , W_a^{\max} are finally used to estimate the mean and extremal values of the damping with the definition Eq (10). The aeroelastic damping therefore oscillates in a bounded interval when multiple perturbations contribute to the aeroelastic response. The definitions proposed here are coherent with those usually employed for periodic responses in which case the aerodynamic work is constant whatever the initial time instant.

5 Numerical results

The previous developments for the generalized aerodynamic forces reconstruction and for the aeroelastic damping predictions have been validated numerically on a contrafan model with $N_{b,0} = 10$ and $N_{b,1} = 14$ blades in each blade row R_0 and R_1 respectively. A vibration is prescribed to the 2^{nd} blade row R_1 with the first torsion eigenmode and the different values of the nodal diameter $n_d = 0, \ldots \pm N_{b,1}/2$. Further details on the configuration can be found in [12].

Numerical computations on a single passage with phase-shifted boundary conditions are compared to reference computations performed on the full 360° annulus for different values of the nodal diameter. The relative errors between the reference local generalized aerodynamic forces computed with the 360° configuration and the single passage model with phase-shifted boundary conditions and $N_p = 2$ spinning modes are listed in the second column of table 1. The agreement is generally good except for some nodal diameters $(n_d = -1;7)$ for which the error is larger (about 30 %) and for the nodal diameter $n_d = 5$ which is poorly approximated. It should be mentioned that the errors may be reduced for some nodal diameters by increasing the number of spinning modes for the field approximation on the boundary conditions (see [12]).

The errors are also given in table 1 for the global generalized aerodynamic forces reconstructed from the expressions Eqs (17) and (21) using either the local generalized aerodynamic forces computed with the 360° model or with the single passage model. The error is very low for most of the nodal diameters (less than 2%). How-

n_d	$oldsymbol{arepsilon}(f_{ag,\mathrm{sp}}^{\mathfrak{R},\Gamma_0})$	$arepsilon(f_{ag,360}^{\mathfrak{R},\Gamma})$	$oldsymbol{arepsilon}(f_{ag,\mathrm{sp}}^{\mathfrak{R},\Gamma})$
0	2.3%	0.01%	0.2%
+1	4.2%	0.01%	1.9%
-1	33.5%	0.00%	41.2%
+2	0.9%	0.02%	0.2%
-2	2.1%	0.01%	0.4%
+3	2.7%	0.01%	0.3%
-3	2.1%	0.01%	1.5%
+4	10.4%	0.02%	0.6%
-4	1.0%	0.02%	0.4%
+5	93.0%	10.20%	204.7%
-5	1.4%	0.24%	0.7%
+6	12.2%	0.11%	7.5%
-6	7.2%	0.03%	5.5%
±7	27.3%	0.02%	25.1%

Table 1: Averaged relative error on the real part of the local generalized aerodynamic force $(f_{ag,sp}^{\mathfrak{R},\Gamma_0})$ computed with the single passage model and of the global generalized aerodynamic force approximated with Eqs (17) and (21) from the local generalized aerodynamic force computed with the 360° model $(f_{ag,360}^{\mathfrak{R},\Gamma})$ or the single passage model $(f_{ag,sp}^{\mathfrak{R},\Gamma})$. Similar errors (not reported here) are found for the imaginary parts.

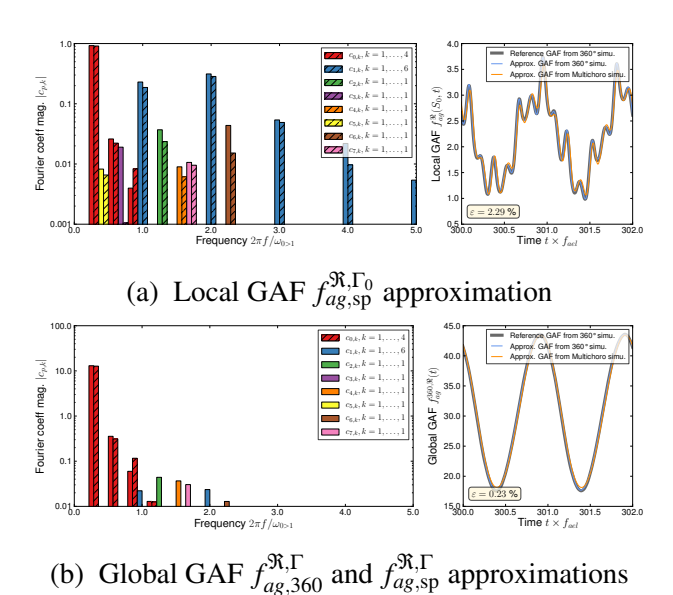


Fig. 1: Comparison of the local and global reconstructed generalized aerodynamic forces for the nodal diameter $n_d = 0$.

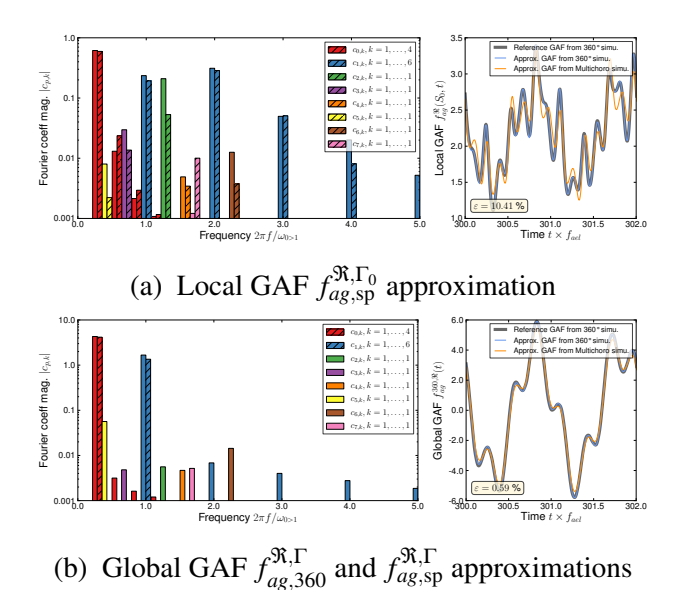


Fig. 2: Comparison of the local and global reconstructed generalized aerodynamic forces for the nodal diameter $n_d = 4$.

ever the nodal diameters $n_d = -1;5$ and 7 for which the local generalized aerodynamic forces were poorly predicted are unsurprisingly large since the approximation (17) is based on an accurate approximation of the local generalized aerodynamic force. The periodicity property does not seem to be appropriate to approximate the generalized aerodynamic forces for the nodal diameter $n_d = 5$ since the error of reconstruction from the local generalized aerodynamic force computed with the 360° model is quite large ($\varepsilon(f_{ag,360}^{\Re,\Gamma}) = 10.2\%$) whereas it is not greater than 0.25% for all other nodal diameters. Investigations are further made to better understand this inaccuracy.

The spectral content and the time histories of the local and global generalized aerodynamic forces are plotted on figures 1 and 2 for the nodal diameters $n_d = 0$ and 4 respectively. The spectra represent the magnitude $c_{p,k}[f_{ag}^{\mathfrak{R},\bullet}] = (a_{p,k}[f_{ag}^{\mathfrak{R},\bullet}] + b_{p,k}[f_{ag}^{\mathfrak{R},\bullet}])^{1/2}$ of the Fourier coefficients of the local or global generalized aerodynamic forces. The following 8 pulsations are considered for the approximation: $\omega_p \in \{\omega_0, \omega_{R_0 \succ R_1}, m\omega_{R_0 \succ R_1} + \ell\omega_0\}$ with $(\ell, m) = (\pm 1, 1)$, $(\pm 2, 1)$ and $(\pm 1, 2)$ and $N_{h,p} = 6$ for $\omega_{R_0 \succ R_1}, N_{h,p} = 4$ for ω_0 and $N_{h,p} = 1$ otherwise. For each pair of bars, the first one is the mag-

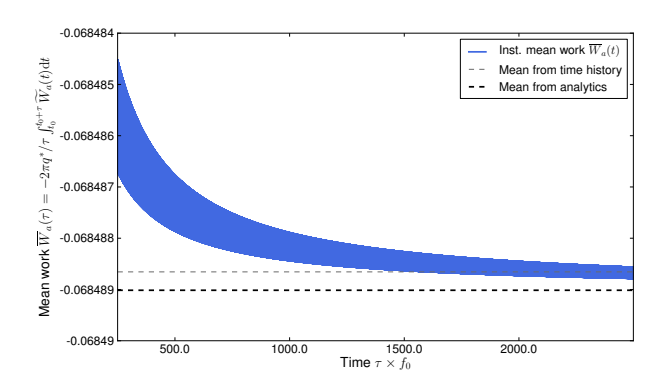


Fig. 3 : Convergence of the mean aerodynamic work \overline{W}_a .

nitude of the reference (local or global) generalized aerodynamic force and the second is the approximation computed with the single passage approach. The spectral content of the global generalized aerodynamic force is strikingly less populated than the one of the local generalized aerodynamic force because of the Dirac comb operator $\coprod_{N_h} (\mathfrak{K}_{n_k}^{\pm})$ which filters out most of the components. The resulting global generalized aerodynamic forces are therefore periodic for some nodal diameters (e.g. $n_d = 0$) but some components are preserved when the condition for the Dirac comb are satisfied: e.g. for $n_d = 4$ the 1st harmonic of the spinning mode related to the blade passage with $\kappa_p = N_{b,0} = 10$ leads to $\mathfrak{K}_{p,k}^+ = n_d + k\kappa_p = 14 \equiv 0 \pmod{N_{b,1}}.$

The convergence of the mean aerodynamic work Eq (22) is illustrated on figure 3 for the nodal diameter $n_d = 4$. The time history is plotted for a time interval 5 times longer than the one computed by the CFD code. This is possible since the Fourier approximation of the generalized aerodynamic forces allows the evaluation for any time interval. The black dashed line is the analytical mean value given by Eq (23) which is reached only for an infinitely long time interval. The grey dashed line represents a "numerical" mean value computed from the evaluation of the integrand on the last 10% of the time history.

The time history of the instantaneous aerodynamic work $W_a(t_0)$ is finally computed using the analytical approximation (24). From this time history evaluated on a very long time interval

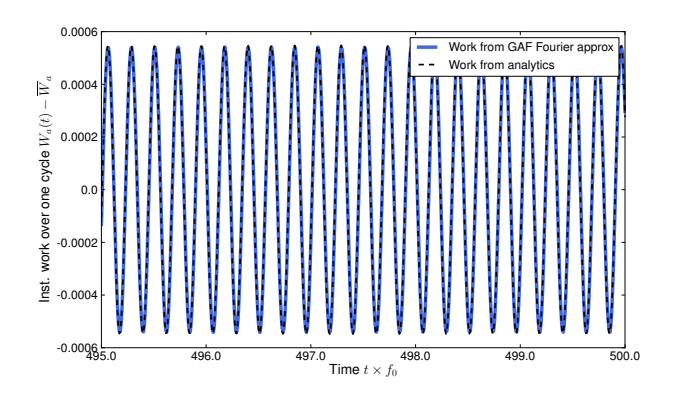


Fig. 4: Comparison of instantaneous aerodynamic work W_a for the nodal diameter $n_d = -4$.

(~ 2500 vibration cycles), a numerical estimate of the extrema and average values of the work are computed. The comparison with the instantaneous aerodynamic work computed from the generalized aerodynamic forces time history is shown on figure 4.

The corresponding aeroelastic damping Eq (10) is evaluated and the result is plotted on figure 5 for all possible nodal diameters. The evolution of the damping is more irregular when the effects of the upstream blade row are taken into account. A large difference is observed for the nodal diameter $n_d = 5$ in which case the stability is significantly reduced. The single passage simulations agree quite well with the damping values computed from the 360° computation except for the nodal diameters $n_d = -1$ and 5 for which the generalized aerodynamic forces approximation was not satisfactory.

6 Conclusion

In this paper single passage simulations with enhanced phased-lagged boundary conditions have been used to evaluate the aeroelastic damping of a contrafan. Such simulations are less time consuming but the generalized aerodynamic forces are computed only on the reference passage modeled. Under the same assumption of space-time periodicity than the one used for the phase-lagged boundary conditions, the global generalized aerodynamic forces of the whole blade row can be approximated analytically and the global stability

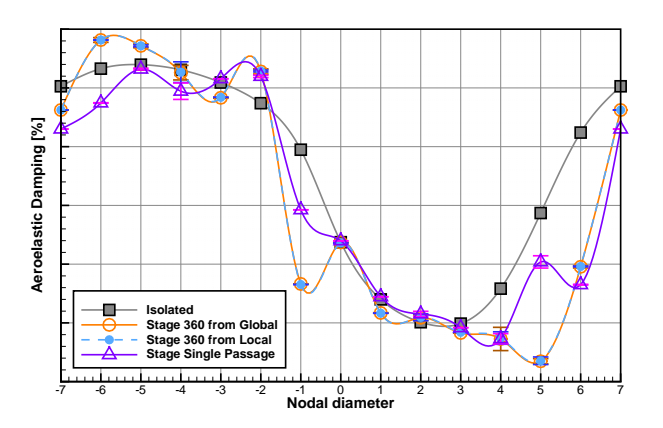


Fig. 5: Comparison of aeroelastic damping on the isolated and stage blade row configurations. Results are plotted for the 360° and single passage stage configurations.

can be assessed. The comparison of the aeroelastic damping values obtained in this way with reference 360° simulations shows a good agreement for most nodal diameters. Besides, the effects of the upstream blade row on the stability have proved to be significant for some nodal diameters. Such a procedure for the aeroelastic damping estimation of turbomachinery bladed disc assemblies may therefore be a good compromise between usual aeroelastic computations on isolated blade row configurations and computationally expensive simulations on 360° configurations.

7 Contact Author Email Address

antoine.placzek@onera.fr

References

- [1] Cambier L, Heib S and Plot S. The Onera elsA CFD software: input from research and feedback from industry. *Mech. & Ind.*, Vol. 14, No. 3, pp 159–74, 2013. doi: 10.1051/meca/2013056.
- [2] Carta F O. Coupled blade-disk-shroud flutter instabilities in turbojet engine rotors. *J. Eng. Gas Turbines Power*, Vol. 89, No. 3, pp 419–426, 1967. doi: 10.1115/1.3616708.
- [3] Castillon L. Evaluation of a multiple frequency phase-lagged method for unsteady nu-

- merical simulations of multistage turbomachinery. 28th Int. Counc. Aeronaut. Sci., Brisbane, 2012. URL www.icas.org/ICAS_ARCHIVE/ICAS2012/PAPERS/056.PDF.
- [4] Dugeai A, Madec A and Sens A S. Numerical unsteady aerodynamics for turbomachinery aeroelasticity. 9th Int. Symp. Unsteady Aerodyn. Aeroacoust. Aeroelast. Turbomach., Lyon, 2000.
- [5] Erdos J I, Alzner E and McNally W. Numerical solution of periodic transonic flow through a fan stage. *AIAA J.*, Vol. 15, No 11, pp 1559–68, 1977. doi: 10.2514/3.60823.
- [6] Gerolymos G A, Michon G J and Neubauer J. Analysis and application of chorochronic periodicity in turbomachinery rotor/stator interaction computations. *AIAA J.*, Vol. 18, No. 6, pp 1139–52, 2002. doi: 10.2514/2.6065.
- [7] He L. Method of simulating unsteady turbomachinery flows with multiple perturbations. AIAA J., Vol. 30, No 11, pp 2730–35, 1992. doi: 10.1016/j.paerosci.2010.04.001.
- [8] Huang X Q, He L and Bell D L. Influence of upstream stator on rotor flutter stability in a low pressure steam turbine stage. *J. Power Energy*, Vol. 220, No. 1, pp 25–35, 2006. doi: 10.1243/095765005X69170.
- [9] Kaul R K and Herrmann G. Free torsional vibrations of an elastic cylinder with laminated periodic structure. *Int. J. Solid. Struct.*, Vol. 12, No. 6, pp 449–66, 1976. doi: 10.1016/0020-7683(76)90021-4.
- [10] Li H D and He L. Blade aerodynamic damping variation with rotor-stator gap: a computational study using single-passage approach. *J. Turbomach.*, Vol. 127, No. 3, pp 573–79, 2005. doi: 10.1115/1.1928932.
- [11] Neubauer J. Aérodynamique 3-D instationnaire des turbomachines axiales multi-étages. PhD thesis, University of Paris 6, 2004. URL julien.neubauer.free.fr/THESE_ JN.pdf.
- [12] Placzek A and Castillon L. Aeroelastic response of a contrafan stage using full annulus and single passage models. *J. Aeroelast*.

- *Struct. Dyn.*, Vol. 3, No. 2, pp 1–30, 2014. doi: 10.3293/asdj.2014.30.
- [13] Saiz G. Turbomachinery aeroelasticity using a time-linearised multi blade-row approach. PhD thesis, University of London, 2008. URL workspace.imperial.ac.uk/medynamics/Public/gaby_saiz_thesis.pdf.
- [14] Silkowski P D and Hall K C. A coupled mode analysis of unsteady multistage flows in turbomachinery. *J. Turbomach.*, Vol. 120, No. 3, pp 410–22, 1998. doi: 10.1115/1.2841732.
- [15] Tyler J M and Soffrin T G. Axial flow compressor noise studies. *SAE Trans.*, Vol. 70, pp 309–32, 1962. doi: 10.4271/620532.
- [16] Valid R and Ohayon R. Théorie et calcul statique et dynamique des structures à symétries cycliques. *Rech. Aérosp.*, Vol. 4, pp 251–63, 1985.

Acknowledgments

This work was supported by the Direction Générale de l'Aviation Civile (DGAC) under the Convention n° 2009 93 0834 for the research project Aerovista. Thanks to SAFRAN (Snecma) for providing the contrafan model.

Copyright Statement

The authors confirm that they, and/or their company or organization, hold copyright on all of the original material included in this paper. The authors also confirm that they have obtained permission, from the copyright holder of any third party material included in this paper, to publish it as part of their paper. The authors confirm that they give permission, or have obtained permission from the copyright holder of this paper, for the publication and distribution of this paper as part of the ICAS 2014 proceedings or as individual off-prints from the proceedings.